

## Formation and decomposition of CO<sub>2</sub>-filled ice

B. Massani, C. Mitterdorfer, and T. Loerting

Citation: *The Journal of Chemical Physics* **147**, 134503 (2017); doi: 10.1063/1.4996270

View online: <http://dx.doi.org/10.1063/1.4996270>

View Table of Contents: <http://aip.scitation.org/toc/jcp/147/13>

Published by the [American Institute of Physics](#)

---

---



**Scilight**

Sharp, quick summaries **illuminating**  
the latest physics research

Sign up for **FREE!**

**AIP**  
Publishing

## Formation and decomposition of CO<sub>2</sub>-filled ice

B. Massani, C. Mitterdorfer, and T. Loerting<sup>a)</sup>

*Institute of Physical Chemistry, University of Innsbruck, Innrain 52c, 6020 Innsbruck, Austria*

(Received 15 July 2017; accepted 12 September 2017; published online 5 October 2017)

Recently it was shown that CO<sub>2</sub>-filled ice is formed upon compression of CO<sub>2</sub>-clathrate hydrate. Here we show two alternative routes of its formation, namely, by decompression of CO<sub>2</sub>/ice VI mixtures at 250 K and by isobaric heating of CO<sub>2</sub>/high-density amorphous ice mixtures at 0.5–1.0 GPa above 200 K. Furthermore, we show that filled ice may either transform into the clathrate at an elevated pressure or decompose to “empty” hexagonal ice at ambient pressure and low temperature. This complements the literature studies in which decomposition to ice VI was favoured at high pressures and low temperatures. © 2017 Author(s). All article content, except where otherwise noted, is licensed under a Creative Commons Attribution (CC BY) license (<http://creativecommons.org/licenses/by/4.0/>). <https://doi.org/10.1063/1.4996270>

### I. INTRODUCTION

The investigation of inclusion compounds such as clathrate hydrate or filled ice at high-pressure conditions is of interest for a fundamental understanding of the interactions in guest-host systems. CO<sub>2</sub>-H<sub>2</sub>O is of importance in a broad range of fields, including astrophysics, geochemistry, marine biology, food chemistry, and medicine. Under high pressure (e.g., in the interior of planets/moons) or upon impact solid mixtures of CO<sub>2</sub>-H<sub>2</sub>O may form clathrate hydrates, filled ice, or carbonic acid.<sup>1–6</sup> The formation of H<sub>2</sub>CO<sub>3</sub> was suggested in 2016 by Saleh and Oganov using computer simulation.<sup>7</sup> Experimentally, H<sub>2</sub>CO<sub>3</sub> was found by Wang *et al.* who performed IR-experiments at high pressures above 2.4 GPa.<sup>6</sup> This compound is surprisingly stable at low temperatures and high pressures.<sup>8</sup>

In cold environments, also mixed compounds such as CO<sub>2</sub>-clathrate hydrates may form. Clathrate hydrates are hydrogen bonded water cages, stabilized by non-covalently bond guest molecules.<sup>1,9–11</sup> Depending on the size of the guest molecule, different crystal structures are formed (e.g., cubic structures CS-I and CS-II and hexagonal structure H).<sup>2</sup> It is worth remarking that carbon dioxide, as a medium sized molecule with an average diameter of about 5 Å, may occupy the small 5<sup>12</sup> cages (consisting of 12 pentagons formed by the H<sub>2</sub>O molecules with oxygen atoms on each corner position) as well as the larger 5<sup>12</sup>6<sup>2</sup> cages (consisting of 12 pentagons and 2 hexagons formed by the H<sub>2</sub>O molecules with oxygen atoms on each corner position) of the CS-I structure.<sup>2</sup> Clathrates can therefore be used to fix large amounts of CO<sub>2</sub>. This type of carbon sequestration may be of environmental interest. Presently many different routes to synthesize clathrate hydrates are known. The most common ones are liquid-liquid, liquid-gas, and solid-gas interface methods.<sup>2,12–15</sup>

Loveday *et al.* first investigated the high-pressure behavior of clathrate hydrates on the example of methane guests: Cubic structure clathrate hydrates transform with increasing pressure into the hexagonal structure.<sup>1</sup> The hexagonal structure changes on pressurization either into the tetragonal structure or into methane hydrate III (MH-III), a filled ice structure.<sup>16,17</sup>

Hirai *et al.* first reported on a new crystalline high pressure phase of CO<sub>2</sub> and H<sub>2</sub>O.<sup>3</sup> Formed by compressing CO<sub>2</sub>-clathrate hydrate type I (space group *Pm3n*)<sup>2</sup> using diamond anvil cells and a helium-refrigeration cryostat, this phase was revealed at pressures above approximately 0.6 GPa and below 1.0 GPa. Above this pressure, the new phase decomposes to dry ice (space group *Pa3̄*)<sup>18</sup> and ice VI (space group *P4<sub>2</sub>/nmc*)<sup>19</sup>. Tulk *et al.* solved the structure of this new phase<sup>20</sup> in 2014 by fitting diffraction data with computer models (space group *Imma*). According to their fundamental work, the structure is similar to MH-III, which itself is remarkably similar to the structure of hexagonal ice (ice *I<sub>h</sub>*, space group *P6<sub>3</sub>/mmc*)<sup>21</sup>: The guest molecules are located in the channels of the H<sub>2</sub>O network. Due to the guests, the structure of filled ice is—compared to ice *I<sub>h</sub>*—stretched and shows larger O–O distances and larger lattice constants. In 2013, Bollengier studied the decomposition behavior of carbon dioxide filled ice at temperatures above 250 K.<sup>4</sup> They found that filled ice decomposes to ice VI and dry ice upon heating to temperatures above ≈270 K. An open question is that why Bollengier *et al.*<sup>4</sup> did not find filled ice at temperatures lower than 250 K, while Hirai *et al.*<sup>3</sup> did. Filled ice structures were formerly only known in systems consisting of cubic ice or ice II lattices in the presence of very small molecules and atoms such as H<sub>2</sub> or noble gases.<sup>22–24</sup>

Other routes to the formation of CO<sub>2</sub> filled ice as well as a careful evaluation of the decomposition of filled ice at different *p/T* combinations are missing in the literature. Therefore, we here investigate the high pressure behavior of CO<sub>2</sub>/H<sub>2</sub>O. We reveal two methods to form CO<sub>2</sub> filled ice: from ice VI<sup>19</sup> and dry ice<sup>25</sup> during decompression and from high-density amorphous (HDA) ice and dry ice by isobaric annealing, using a combination of dilatometry, powder X-ray diffraction, and

<sup>a)</sup>Electronic mail: thomas.loerting@uibk.ac.at

calorimetry. Using these approaches, we observe filled ice in a broader pressure range than known before. Furthermore, we reveal that filled ice may either transform into the clathrate or decompose to hexagonal ice and CO<sub>2</sub>, while Bollengier *et al.* observed only ice VI and CO<sub>2</sub>.

## II. MATERIALS AND METHODS

Filled ice is formed by pressurising a vapor-deposit of CO<sub>2</sub>-H<sub>2</sub>O. The vapor co-deposit of H<sub>2</sub>O and CO<sub>2</sub> was produced at 77 K. A scheme of the deposition apparatus is depicted in Fig. 2 in the work of Mayer and Pletzer.<sup>26</sup> The process of the co-deposition was described by Mitterdorfer *et al.* in 2011.<sup>27</sup> In brief, water vapour and gaseous CO<sub>2</sub> enter a high-vacuum chamber via two fine metering valves through a copper tube with a diameter of 13 mm. The inlet pressures for CO<sub>2</sub>/H<sub>2</sub>O were chosen at a ratio of 1:10, namely, the pressure for CO<sub>2</sub> is 0.02 mbar and for H<sub>2</sub>O is 0.2 mbar (background pressure 10<sup>-4</sup> mbar). The two gases are deposited on a copper plate kept at 77 K (deposition time ≈12 h). The deposit of roughly 2 mm in thickness is recovered at ambient pressure by scratching it off the copper plate and stored under liquid nitrogen.

The deposit was characterised *ex situ* by powder X-ray diffraction (XRD). To that end, the samples were cold-loaded under liquid nitrogen to the cold (77 K) sample holder in the XRD-chamber (*Anton Paar TTK450*). Diffractograms were recorded at 77 K in the range 15° < 2Θ < 55° at approximately 10<sup>-1</sup> mbar using Cu-K<sub>α</sub> radiation (1.541 Å), following the standard procedure employed in many studies in the past by our group with the X-ray apparatus *Siemens D5000*.<sup>28</sup> The phase compositions of crystalline samples containing more than one specimen were determined using the program *Powder-Cell* (version 2.4, BAM, Bundesanstalt fuer Materialforschung

und -pruefung, Berlin, Germany). An X-ray diffractogram of the co-deposit is shown in Fig. 1(i) and can be compared with Fig. 1(B) in the work of Mitterdorfer *et al.*<sup>27</sup> A broad halo peak between 20° and 32° and several sharp Bragg peaks are visible: the former indicates microporous amorphous solid water (ASW)<sup>29</sup> and is superimposed by the latter indicating crystalline CO<sub>2</sub>.<sup>30</sup>

After the co-deposition experiment and X-ray characterisation, the ice powder was transferred under liquid nitrogen to our piston-cylinder setup. Figure 1 in the work of Elsaesser *et al.*<sup>31</sup> illustrates the experimental setup of our piston-cylinder apparatus. The ice powder was filled into the 8 mm bore of the hardened steel cylinder, where an indium lining acts as a lubricant.<sup>32,33</sup> Without lubricant, pressure drops and shock-wave heating occur in the sample and may lead to crystallisation.<sup>33</sup> The loose ice powder was then precompacted to a cylinder shape by applying a pressure of 0.2 GPa<sup>30</sup> and used as the starting material for all further experiments carried out. They are marked by (i) in the piston displacement curves shown in Fig. 2; the respective powder diffractogram is shown in Fig. 1(i). These samples were then used to conduct compression/decompression cycles including a high-pressure annealing step. Specifically, the samples were compressed at 77 K to 1.8 GPa and then heated isobarically to 200 or 250 K with a heating rate of 3 K/min. The samples were then quench recovered or isothermally decompressed at 200 or 250 K to selected pressures (0.02–0.8 GPa) before quench recovery.

The quench-recovered specimens were analyzed by X-ray diffraction,<sup>30,33</sup> and some selected specimens were additionally investigated by differential scanning calorimetry (DSC). DSC experiments were carried out using DSC8000 (PerkinElmer) at ambient pressure and heating rates between 3 and 30 K min<sup>-1</sup>. Samples were placed in an aluminium

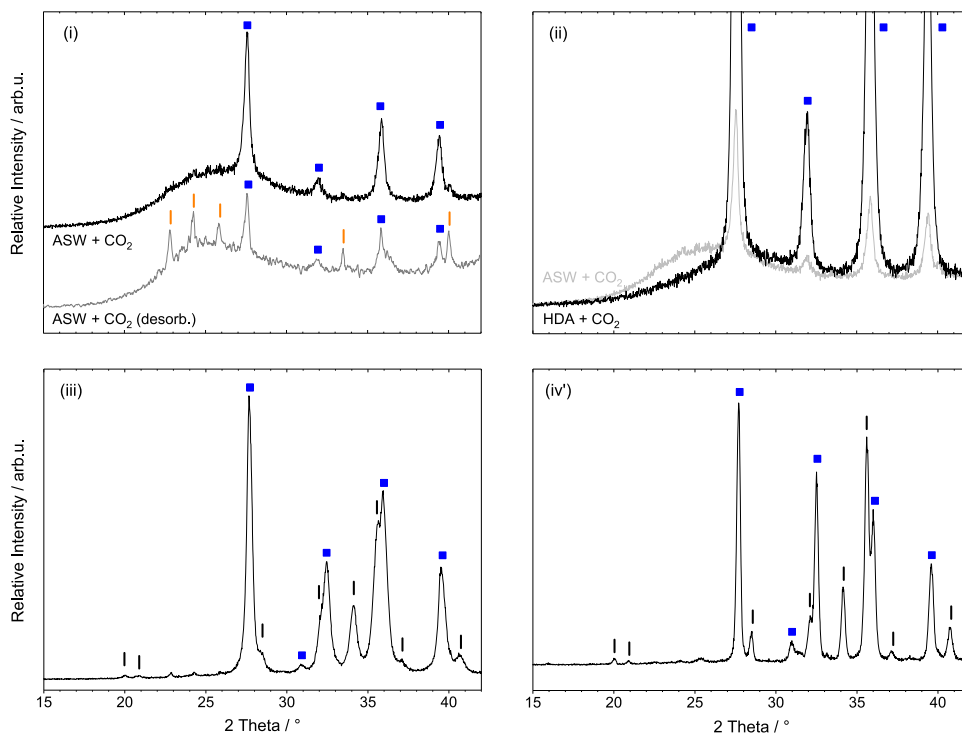


FIG. 1. (i) XRD scan of ASW-CO<sub>2</sub> co-deposit. The black curve shows a sample that was not heated above 77 K. The grey curve shows a sample that was heated in the deposition apparatus to 130 K. Upon this heating, the surface CO<sub>2</sub> desorbs. The orange labeled reflections (ice I<sub>h</sub>) indicate condensed water from air. (ii) Sample after the compression to 1.8 GPa. The maximum of the halo peak is shifted to larger angles, compared to ASW, indicating the transformation to HDA. (iii) Sample after compression to 1.8 GPa and annealing to 195 K. (iv') Sample after compression to 1.8 GPa and annealing to 250 K. The blue squares, orange dashes, and black dashes represent Bragg peaks of dry ice, ice I, and ice VI, respectively.

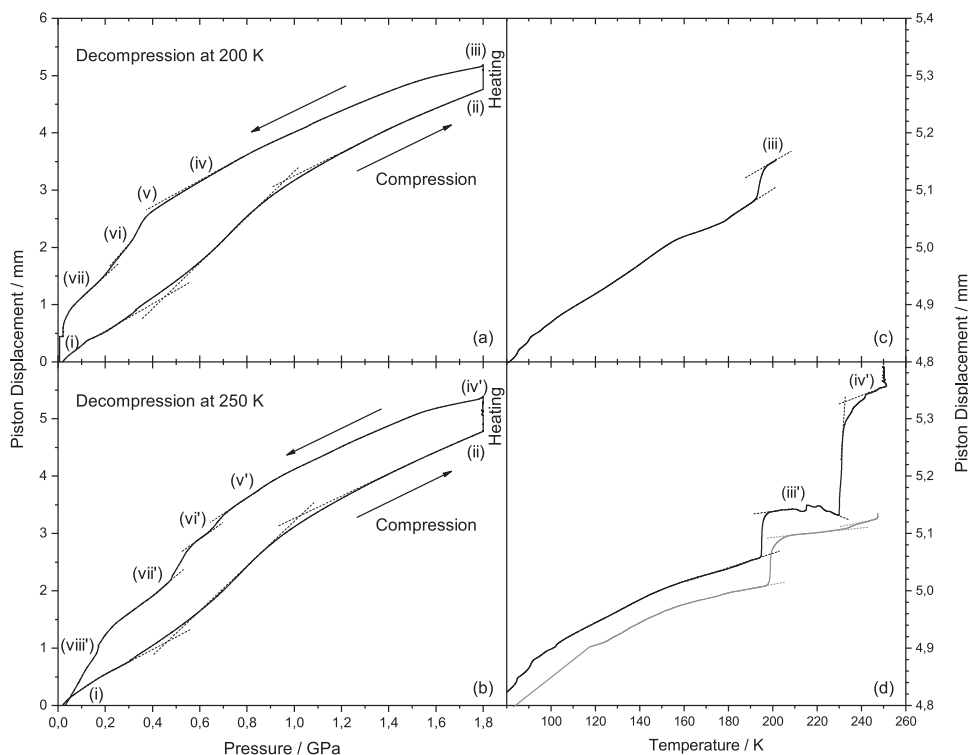


FIG. 2. Piston displacement curves of (a) and (b) compression at 77 K, (b) and (c) isobaric heating at 1.8 GPa and decompression at 200 K (a) and 250 K (b), respectively. A piston displacement in the upward direction is equivalent to the densification of the sample. The sample mass cannot be determined accurately based on weighing. However, from the size of the densification steps, we estimate the sample mass to be on the order of 200 mg.

crucible, which was closed with a lid. During this, the samples were kept under liquid nitrogen.

### III. RESULTS

#### A. Formation of the filled ice—Decompression of ice VI and solid CO<sub>2</sub>

Figure 2 reports a volumetric experiment on the CO<sub>2</sub>/H<sub>2</sub>O co-deposit. Point (i) in panels (a) and (b) represents the vapor co-deposit of carbon dioxide and amorphous solid water (ASW + crystalline CO<sub>2</sub> with the space group  $Pa\bar{3}$ )<sup>18</sup> after the transfer to the piston-cylinder setup at 77 K and precompaction. The respective diffractogram is shown in Fig. 1(i). Upon compression, a step in density is seen between 0.4 GPa and 1.1 GPa. This corresponds to the well known polyamorphic transformation of ASW to high-density amorphous (HDA) ice. This was reported first by Mishima in 1994 on the example of pure low-density amorphous (LDA) ice.<sup>34</sup> As compared to pure LDA ice, the step is about 0.1 GPa broader for CO<sub>2</sub>/H<sub>2</sub>O.<sup>35</sup> Thus, at point (ii), the samples consist of CO<sub>2</sub>(s) and HDA ice. The transformation can be recognised in Fig. 1(ii), in which a shift of the broad halo peak to higher angles is seen. For comparison, the halo peak before compression is shown in light colour in Fig. 1(ii). From the step height, we can estimate in hindsight that we had loaded approximately 200 mg of ASW, not considering the additional mass of crystalline CO<sub>2</sub>. This corresponds roughly to a cylinder of 8 mm in diameter and 10 mm in height.

Isobaric heating at 1.8 GPa to 200 K leads to crystallization of HDA ice to ice VI,<sup>36–38</sup> which can be observed in the decrease of volume around 195 K in Figs. 2(c) and 2(d). Therefore, the diffractogram of the quench-recovered specimen in

Fig. 1(iii) reveals a mixture of crystalline CO<sub>2</sub> and ice VI. Upon continued heating, a second step is observed at about 230 K in Fig. 2(d). The positive value of the piston displacement indicates a loss of volume.

The height of this second step is dependent on the amount of carbon dioxide in the sample: The grey curve in Fig. 2(d) shows an experiment performed with a co-deposit that was heated in the deposition apparatus to 130 K. At that temperature, the excess CO<sub>2</sub> adsorbed on the external surface of the sample desorbs, whereas it remains on the internal pore surfaces. A diffractogram of such a co-deposit after heating *in vacuum* is shown in Fig. 1(i) (grey diffractogram). Since the height of this step is dependent on the amount of CO<sub>2</sub> in the starting material, this decrease of volume is assigned to the thermal desorption of CO<sub>2</sub> from the ice surface: carbon dioxide above 230 K shows an increased mobility. The desorbed CO<sub>2</sub> then leaves the piston cylinder instrument, which is not gas tight.

The samples in Figs. 1(iii) and 1(iv') consist therefore of ice VI and solid carbon dioxide entrapped in an ice matrix. The respective diffractograms are shown in Figs. 1(iii) and 1(iv'), respectively.

Also during the decompression, the piston displacement curves exhibit steps, which are indicative of phase changes to lower dense phases. For the decompression at 200 K [starting from point (iii) in Fig. 2(a)], a single step is found between 0.4 and 0.3 GPa. In the case of the 250 K experiment (starting from (iv'), in Fig. 2(b), there are two steps located between 0.8 and 0.6 GPa as well as 0.6 and 0.4 GPa. A final step at <0.2 GPa is seen both in Figs. 2(a) and 2(b). The XRD scans after quench-recovery from the points marked in Figs. 2(a) and 2(b) are given in Fig. 3 for the decompression at 200 K and 250 K, respectively.

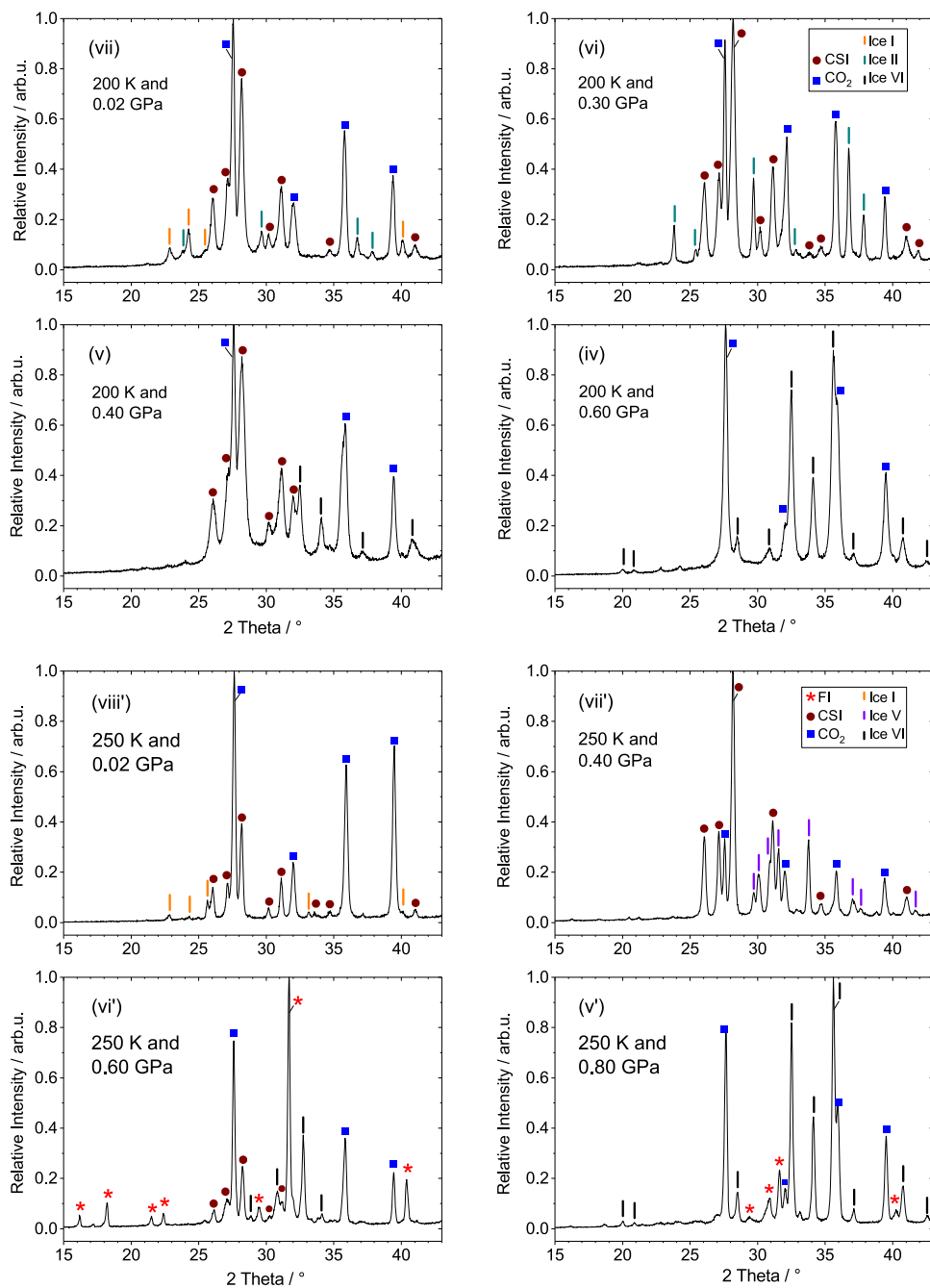
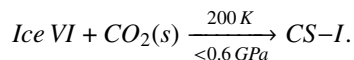


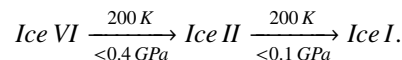
FIG. 3. Top: Powder X-ray diffractograms for isothermal decompression at 200 K and quench-recovery at 0.02 GPa, 0.3 GPa, 0.4 GPa, and 0.6 GPa [curves (a) and (c) in Fig. 2]. Bottom: Powder X-ray diffractograms for isothermal decompression at 250 K and quench-recovery at 0.02 GPa, 0.4 GPa, 0.6 GPa, and 0.8 GPa [curves (b) and (d) in Fig. 2].

At 200 K and 0.6 GPa, see Fig. 3(iv), crystalline CO<sub>2</sub> and ice VI are still the two dominant phases. Decompression to <0.4 GPa, Fig. 3(v), leads to the formation of the cubic clathrate hydrate type I (CS-I), with crystalline carbon dioxide and ice VI still being present. The most prominent Bragg peak of ice VI at 35.6° vanishes, whereas the Bragg peak of CS-I hydrate at 28.5° becomes the most intense one. Thus, the CO<sub>2</sub>-ice VI mixture transforms directly into the clathrate hydrate,



Both CO<sub>2</sub> and ice VI were not completely transformed and remain partly in the sample. However, whereas large amounts of solid carbon dioxide remain, only small amounts of ice VI remain.

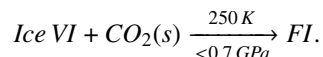
At 200 K and 0.3 GPa, Fig. 3(vi), besides the clathrate, ice II is also observed. That is, the remainder of ice VI in (v) has transformed to ice II in Fig. 3(vi), e.g., peaks at 24°, 37°, and 38° grow. Further decompression to 0.02 GPa results in the observation of hexagonal ice in Fig. 3(vii) due to the transformation of ice II to hexagonal ice. The remaining ice VI undergoes phase transitions upon decompressing according to the phase diagram of water,



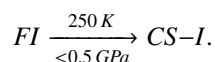
Both the CO<sub>2</sub>-clathrate and CO<sub>2</sub>(s) remain stable down to 0.02 GPa and 200 K.

At 250 K the evolution of phases is slightly different: At 0.8 GPa and 250 K, Fig. 3(v'), the Bragg peaks originate

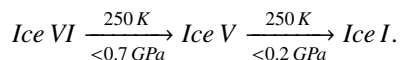
mainly from ice VI and crystalline CO<sub>2</sub> just like at 200 K. However, after the first step in Fig. 2(b), a new phase emerges in Fig. 3(vi'): Reflections attributed to CO<sub>2</sub>-filled ice (FI) appear, namely, 40.4°, 31.7°, 29.5°, 22.4°, 21.5°, 18.2°, and 16.2°<sup>33</sup> at 0.6 GPa and 250 K, Fig. 3(vi'). Additionally, crystalline CO<sub>2</sub> and ice VI remain, and a small amount of clathrate hydrate cubic structure I is formed,



Further decompression beyond the second step in Fig. 2(b) to 0.4 GPa and 250 K, Fig. 3(vii'), leads mainly to the formation of clathrate hydrate CS-I and some ice V, whereby filled ice has completely vanished,



Quench recovery at 0.02 GPa features clathrate hydrate CS-I and solid CO<sub>2</sub> as the main components, Fig. 3(viii'). However, the CS-I hydrate reflections shrink at the expense of the CO<sub>2</sub>(s) reflections: The clathrate hydrate decomposes to ice I and solid CO<sub>2</sub>.<sup>39</sup> The presence of ice V and ice I is a result of the transformation of excess ice VI during the decompression at 250 K according to the phase diagram of water,



The most important difference between these two decompression experiments is the presence of filled ice in the case of 250 K, whereas at 200 K, it is not emerging. The thermal desorption of surface CO<sub>2</sub> and the increased mobility of carbon dioxide, if heated to 250 K, seem to be essential for the formation of filled ice.

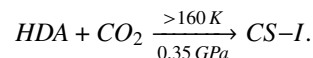
Note that the FI transforms to the clathrate for decompression at 250 K. This is the reverse of the formation mechanism reported by Hirai *et al.*<sup>3</sup>

## B. Formation of the filled ice—Heating HDA and solid CO<sub>2</sub>

In our experiments above, we gave evidence that filled ice is formed by decompression at 250 K but not at 200 K from CO<sub>2</sub>-H<sub>2</sub>O. Hirai *et al.* showed that filled ice may be formed by compression of CS-I at lower temperatures,<sup>3</sup> down to 100 K.

Besides those two ways, we formed filled ice from solid carbon dioxide and HDA by isobaric heating: Here we compressed the co-deposit of carbon dioxide and water to 1.2 GPa to form a mixture of HDA ice and solid carbon dioxide in our piston and cylinder setup at a temperature of 77 K. The sample was then decompressed to various pressures between 0.35 GPa and 1.0 GPa and heated to 230 K. In Fig. 4, the dilatometric curves for the heating steps are depicted.

At 0.35 GPa, only two phase transitions were observed: one at 141 K and the other at 160 K. The sharp step at 141 K is assigned to the crystallisation of HDA ice according to the phase diagram of water.<sup>40</sup> After the second step, the quench-recovered sample consists solely of clathrate hydrate—no filled ice forms at 0.35 GPa,



At higher pressures, more steps are observed, the first one at roughly 160 K. Right after this step, the sample was quench recovered and analyzed by X-ray diffraction. A diffractogram at this temperature is depicted in Fig. 5(a). A broad halo peak at 30° gives evidence that HDA ice is still present. Furthermore, reflections of carbon dioxide are visible as well as emerging Bragg peaks of CO<sub>2</sub>-clathrate hydrate and hexagonal ice.

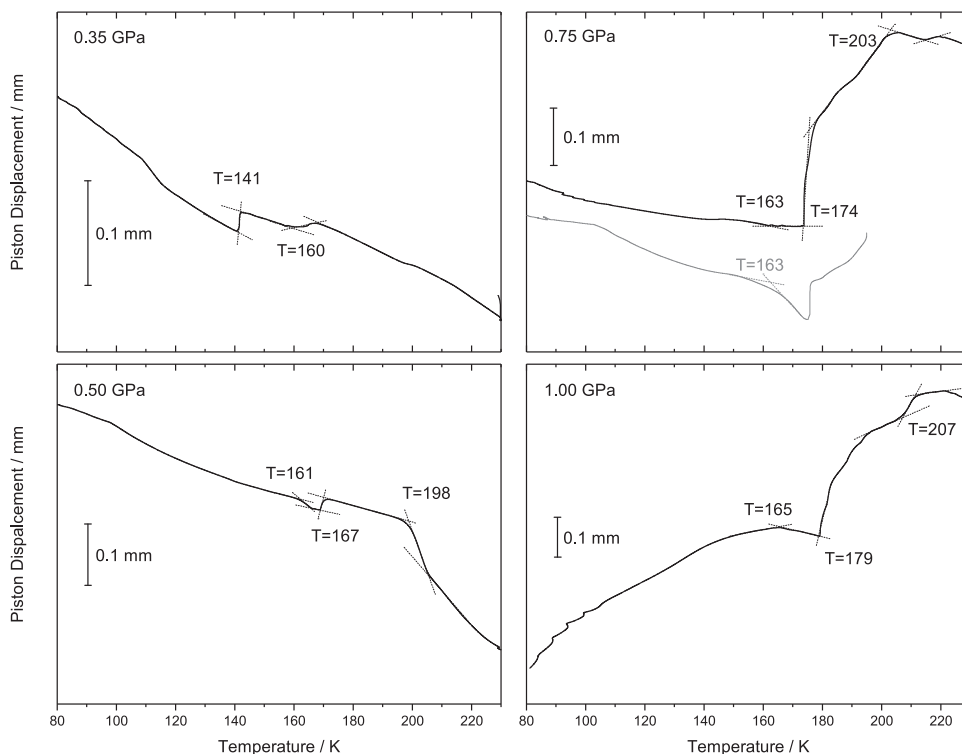


FIG. 4. Dilatometric curves of isobaric annealing of HDA ice and CO<sub>2</sub>(s) in the pressure range between 0.35 GPa and 1.0 GPa.

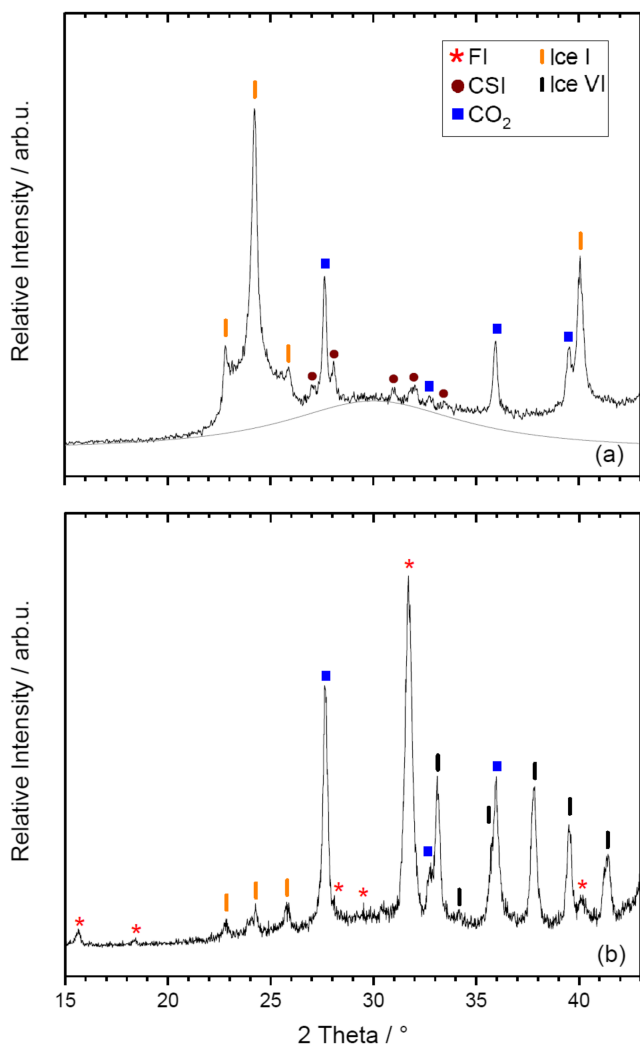
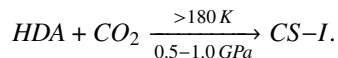


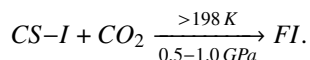
FIG. 5. Examples of the XRD scans of the quench-recovered sample at 165 K (a) and at 230 K (b).

Upon further heating, a sharp step with an onset at 167 K, 174 K, and 179 K occurred at 0.5 GPa, 0.75 GPa, and 1.00 GPa, respectively. This step is assigned to the crystallisation of HDA ice (cf. Stern and Loerting<sup>41</sup>). Compared to pure water, this step is shifted to slightly higher temperatures by about 7 to 8 K. After this step, the clathrate has been formed,



At a temperature of 198 K, 203 K, and 207 K, at 0.50 GPa, 0.75 GPa, and 1.00 GPa, respectively, another step can be observed in the piston displacement curves in Fig. 4. This step is missing in the experiment at 0.35 GPa.

Figure 5(b) shows a respective XRD pattern of the quench-recovered samples at 230 K. Here, the sample consists mainly of filled ice (red \*) together with large amounts of ice VI and solid carbon dioxide. At this temperature, no clathrate hydrate can be observed. The step at  $\approx 200$  K can therefore be assigned to the formation of filled ice from the clathrate hydrate and  $\text{CO}_2(\text{s})$ ,



Here, no direct transition from an amorphous solid to the filled ice is observed. In fact, filled ice is formed at the expense of the clathrate hydrate.

These experiments reveal one major thing: At temperatures above 230 K and 0.5 GPa, all pathways lead to the formation of filled ice. However, at 200 K, it depends on the pathway whether or not filled ice forms, e.g., at 0.5 GPa. In other experiments, it forms in the isobaric heating experiments, but not in the isothermal decompression experiments.

### C. Decomposition of filled ice at 1 bar

The decomposition of  $\text{CO}_2$ -filled ice at high pressures has been previously studied by Hirai *et al.* and by Bollengier *et al.*<sup>3,4</sup> They observed decomposition to ice VI/dry ice and to CS-I. In Sec. III A, we have shown that filled ice transforms to CS-I upon decompression at 250 K. In this subsection, we are going to describe the stability of filled ice using DSC and XRD experiments at ambient pressure (heating rates  $3 \text{ K min}^{-1}$  and  $30 \text{ K min}^{-1}$ , respectively).

The first heating scan in Fig. 6(a) shows two peaks in the calorimetric experiment: a very broad, smeared exotherm between about 105 K and 145 K and a sharp peak with an onset temperature of about 150 K (at  $3 \text{ K min}^{-1}$ ). We attribute the first exotherm to the decomposition of  $\text{CO}_2$ -filled ice. The very broad and also smeared features indicate a very slow transition. The second exothermic peak at 150 K is the well known formation of ice  $I_c$  from high-pressure ice phases, which was first observed calorimetrically by Handa *et al.* in 1988.<sup>42</sup>

In order to determine whether or not the transition is reversible, a second DSC experiment was performed: Fig. 6(b) shows two subsequent heating scans with a heating rate of  $30 \text{ K min}^{-1}$ : first to 140 K and then from 90 K to 160 K. Also in this case, the broad exothermic peak is clearly visible between 100 K and 140 K in the first scan. However, the exotherm disappears to a large extent in the second heating cycle, i.e., the transition is not reversible. The shift of the onset temperature from 109 K at 3 K/min to 100 K at 30 K/min is unexpected.

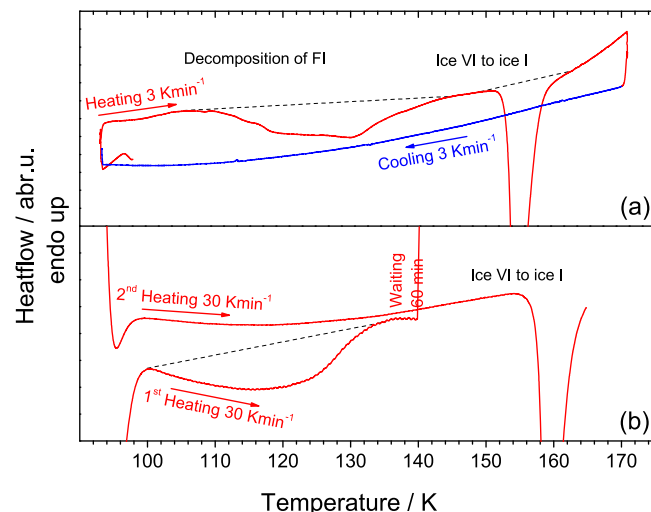


FIG. 6. Top: DSC scan of the quench-recovered specimen with a heating rate of  $3 \text{ K min}^{-1}$ . Bottom: The quench-recovered specimen was heated to 140 K, cooled to 90 K, and heated once again with a heating rate of  $30 \text{ K min}^{-1}$ .

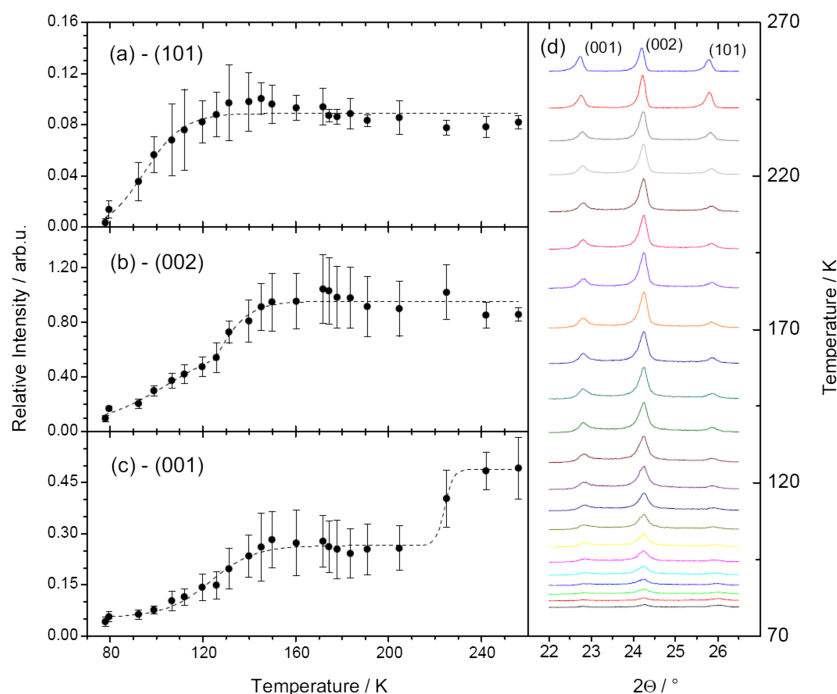


FIG. 7. (a)–(c) The (101), (002), and (001) Bragg peak heights of ice  $I_h$  plotted against the temperature. (d) The corresponding powder X-ray scans between  $22.0^\circ$  and  $26.5^\circ$ . (For the experiment, a heating rate of  $3 \text{ K min}^{-1}$  was used.)

Two samples from two different co-depositions were used and so different degrees of filling might be at its origin.

Possible decomposition products for filled ice at ambient pressure are CS-I hydrate (as noticed above for the decompression experiment at 250 K), ice  $I_c$ , and  $I_h$  (as well as solid  $\text{CO}_2$ ). To investigate this, X-ray diffraction (XRD) experiments were performed in this temperature range: The quench-recovered filled ice was transferred onto a sample holder in a vacuum chamber. This sample holder was slowly heated with a heating rate of  $3 \text{ K min}^{-1}$  to match the rate used for the DSC experiments [Fig. 6(a)]. Bragg peaks were recorded in three different intervals, namely,  $22.0\text{--}26.5^\circ$ ,  $30.0\text{--}33.5^\circ$ , and  $35.0\text{--}36.5^\circ$ . The first interval contains the three most intense ice  $I_h$  Bragg peaks [see Fig. 7(d)]. The second contains the most intense reflections of ice VI,  $\text{CO}_2$ -clathrate hydrate, and  $\text{CO}_2$ -filled ice. Crystalline  $\text{CO}_2$  is found in the third interval. The XRD-patterns plotted against the temperature are given in Fig. 8.

It is clearly visible that the Bragg-peak intensities of ice VI, crystalline carbon dioxide, and filled ice decrease with temperature, whereas the intensities of ice  $I_h$ 's Bragg peaks increase steadily. Compared to that, the intensity of the Bragg peak of cubic type I clathrate hydrate remains relatively constant; hence, the possibility of clathrate hydrate formation during the decomposition of filled ice can be excluded. The respective relative Bragg-peak intensities of ice I [relative to the (002)-peak intensity of hexagonal ice at 230 K] plotted against the temperature are shown in Fig. 7.

Hereby, the Bragg peak at  $26.0^\circ$  reflects the lattice plane (101) and can be found in hexagonal ice only. The most intense of those three reflections is the (002) peak in ice  $I_h$  at  $24.2^\circ$ . It occurs in the diffraction patterns of hexagonal as well as the cubic type ice  $I_c$ . In contrast, the Bragg peak of the lattice plane (001) at  $22.7^\circ$  is more complicated. It is also experimentally observed in patterns of ice  $I_c$  and represents

a measure of hexagonal stacking faults. The more hexagonal stacking faults<sup>44–46</sup> are incorporated in cubic ice, and the more “hexagonal” the ice gets, the more intense this peak becomes.

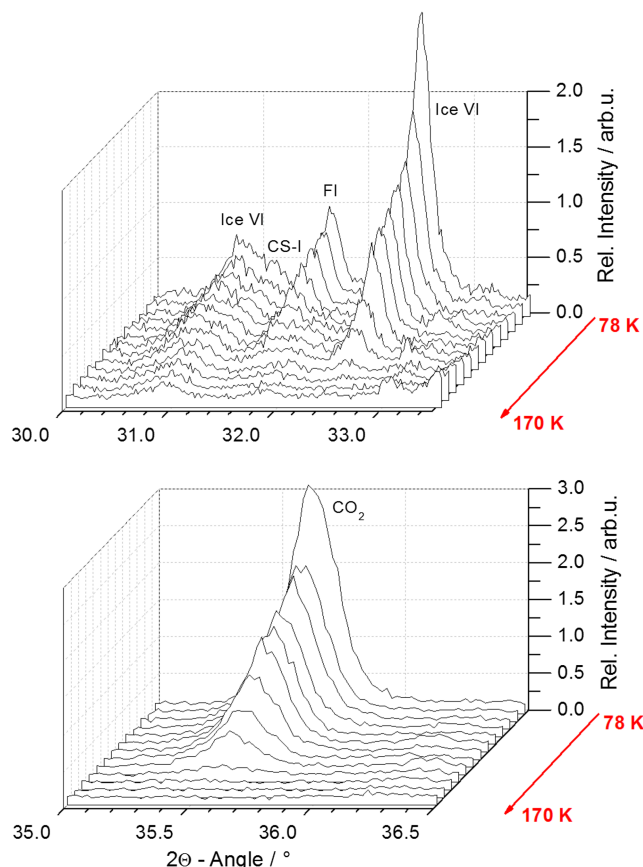


FIG. 8. Top: XRD scan between  $30.0^\circ$  and  $33.5^\circ$  with the most intense reflections of ice VI,  $\text{CO}_2$ -clathrate hydrate, and  $\text{CO}_2$ -filled ice. Bottom: *In situ* XRD scan of the interval of  $35.0^\circ$ – $36.5^\circ$ , containing a reflection of crystalline  $\text{CO}_2$ . A heating rate of  $3 \text{ K min}^{-1}$  was used.

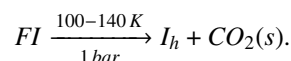
The transition from mainly cubic ice to hexagonal ice usually occurs at around 200 K.<sup>44</sup>

The (002) reflection grows between 100 K and 160 K where it reaches its maximum intensity [see Fig. 7(b)]. After that point, no more ice I is formed. One may even notice two steps, namely, between 100 K and 140 K and between 140 K and 160 K, consistent with the two exotherms in Fig. 6(a). That is, ice I forms both from filled ice and ice VI. Whether ice  $I_c$  or ice  $I_h$  forms from filled ice is answered in Fig. 7(a): There we clearly see that the intensity of the (101)-peak grows between 90 K and 140 K. This indicates that hexagonal ice is formed from filled ice. This is an unusual behavior since high pressure ices usually form cubic ice upon heating.

At last, the Bragg-peak intensities in Fig. 7(c) provide us with the (001) reflections. In this plot, we see two increases of the intensity: the first between 90 K and 140 K and the other one between 200 K and 220 K. The first increase is identical with the rise given in Fig. 7(a), which also indicates that hexagonal ice is formed from filled ice. The second plateau is reached after the remaining cubic ice (formed from ice VI) is transformed into  $I_h$ .

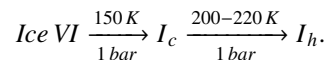
The quench-recovered sample gets “more hexagonal” in exactly the same temperature range as in which filled ice is decomposed. Additionally to that, we see in Fig. 8 that the crystalline  $\text{CO}_2$  is removed from the sample in the very exact temperature range. Hence we conclude that filled ice directly transforms into hexagonal ice by the release of  $\text{CO}_2$  from the

filled channels,



This slow process of  $\text{CO}_2$  release also explains the slow transition observed in our DSC experiments.

Additionally to that, we have the formation of cubic ice from ice VI, which itself is transformed into hexagonal ice at 220 K,



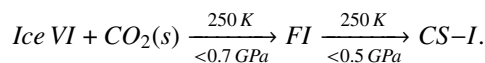
The temperature dependence of the Bragg peak positions as a measure of ice lattice constants is depicted in Fig. 9. In this figure, the filled symbols were measured by us, whereas the open symbols were measured by Roettger *et al.* in 1994.<sup>21</sup> According to Roettger’s studies, water’s lattice constant usually becomes larger upon heating due to the expansion of its primitive cell at temperatures  $>75$  K. The behavior of our samples at temperatures  $>140$  K fits with Roettger’s data quite well. (The larger standard deviation of our data is due to Roettger using single crystals rather than a powder.) However, in the temperature range between 80 K and 140 K, we clearly see that our data points in Fig. 9 shifted to larger angles for the (001) and (101) reflections. This indicates a shift in the lattice constant in the precise temperature range in which filled ice decomposes and therefore also fortifies our explanations. We attribute the deviation from the hexagonal ice data by Rettger *et al.*<sup>21</sup> to the transformation from filled ice (space group  $Imma$ )<sup>20</sup> to hexagonal ice (space group  $P6_3/mmc$ )<sup>21</sup>.

#### IV. CONCLUSIONS

The existence of  $\text{CO}_2$ -filled ice was only discovered recently. Hirai *et al.* were the first to report on a novel but uncharacterized high-pressure phase in the  $\text{CO}_2/\text{H}_2\text{O}$  system in 2010.<sup>3</sup> Only in 2014 it was recognized by Tulk *et al.* that this high-pressure phase is in fact a filled ice based on the hexagonal ice structure.<sup>20</sup> Bollengier *et al.* investigated the stability of filled ice at temperatures  $>250$  K in 2013.<sup>4</sup>

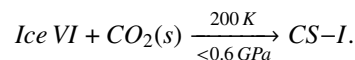
In this work, we here show two alternate routes to form  $\text{CO}_2$ -filled ice. Furthermore, we investigate the decomposition of filled ice at elevated and ambient pressures.

Carbon dioxide filled ice can be formed directly by the decomposition of ice VI and solid  $\text{CO}_2$  from 1.8 GPa at 250 K to 0.6 GPa,



Upon further decompression, filled ice forms clathrate hydrate type I.

However, decompression at a temperature of 200 K leads to the formation of clathrate hydrate with no filled ice being formed,



That is, a previously unknown route towards filled ice has been revealed in our work. We speculate an increased mobility of the carbon dioxide molecules at 250 K which start to desorb from the ice at temperatures  $>230$  K to be at the origin of the filled ice formation.

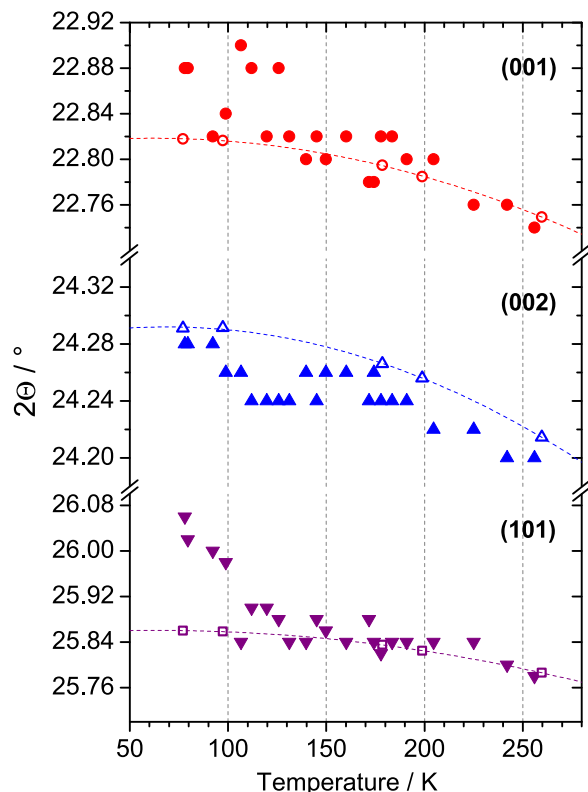
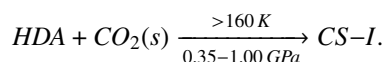
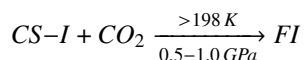


FIG. 9. The filled symbols give the positions of the most intense Bragg peaks observed in the course of the decomposition of  $\text{CO}_2$ -filled ice at ambient pressure plotted against the temperature. The open symbols as well as the dashed lines show the data measured by Roettger *et al.* in 1994 for the lattice planes (100), (002), and (101) of hexagonal ice.<sup>21</sup>

Besides that, filled ice was formed by isobaric heating of high-density amorphous ice and solid carbon dioxide. Upon annealing, first HDA-CO<sub>2</sub> transforms to clathrate hydrate,



Upon further heating, the remaining HDA ice crystallises according to the phase diagram of water. At temperatures above  $\approx 200$  K, once again filled ice is formed with the clathrate hydrate vanishing from the sample. A transformation



is the reason for this. In the decompression experiments, at this very temperature, no filled ice was observed. Also, Bollengier *et al.*<sup>4</sup> did not find filled ice at that temperature. That is, the formation of filled ice is strongly dependent on the pathway. It forms much more readily from the CO<sub>2</sub> clathrate than from ice VI/CO<sub>2</sub>.

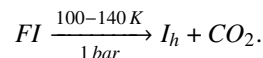
All experiments carried out are summarised in Fig. 10. Also selected data points from Hirai *et al.*<sup>3</sup> and Bollengier *et al.*<sup>4</sup> are depicted.

In this figure, the grey line corresponds to the crystallisation temperatures of the amorphous water phases. The orange line is the melting curve of clathrate hydrate. The dotted red line gives the proposed stability region of carbon dioxide filled ice as given by Hirai *et al.*

We found filled ice at lower as well as higher pressures. This may be due to us using a macroscopic amount of the sample (200 mg), whereas Hirai *et al.*<sup>3</sup> only studied filled ice in diamond anvil cells with much smaller samples. Furthermore, this may also be due to different mixing ratios between CO<sub>2</sub> and H<sub>2</sub>O in different sets of experiments. Since the mixing ratios are not known from our experiments, they are not explicitly included in Fig. 10.

At ambient pressure, filled ice does not transform to CS-I as it does at high-pressure but releases gas and directly transforms into hexagonal ice in a temperature range between 100 K

and 140 K. High-pressure ice is usually converted to cubic ice not hexagonal ice first at ambient pressure. Here, the structural similarity between I<sub>h</sub> and FI leads to a direct transformation to hexagonal ice,



During this process, the CO<sub>2</sub> is released from the channels, resulting in solid CO<sub>2</sub>. These results are not only novel from the experimental perspective but also represent a benchmark for theoretical studies. For example, the formation of the CS-I clathrate from filled ice as well as the absence of carbonic acid near 1 GPa provides strict constraints on the intermolecular potentials governing the CO<sub>2</sub>/H<sub>2</sub>O systems.

*Note added in proof.* Very recently a publication by Amos *et al.* appeared [Daniel M. Amos, Mary-Ellen Donnelly, Pattanasak Teeratchanan, Craig L. Bull, Andrzej Falenty, Werner F. Kuhs, Andreas Hermann, and John S. Loveday, A Chiral Gas-Hydrate Structure Common to the Carbon Dioxide-Water and Hydrogen-Water Systems, *J. Phys. Chem. Lett.* **8**, 4295–4299 (2017)], in which the filled ice was actually shown to be of a more complex, chiral structure based on neither a known hydrate nor ice structure but instead related to two Zintl phases. Therefore, our finding is surprising that this high pressure hydrate of CO<sub>2</sub> transforms into hexagonal ice rather than cubic ice at ambient pressure.

## ACKNOWLEDGMENTS

We gratefully acknowledge funding of the study from the Austrian Science Fund (FWF), Project Nos. P18187 and I1392. The authors declare no competing financial interest.

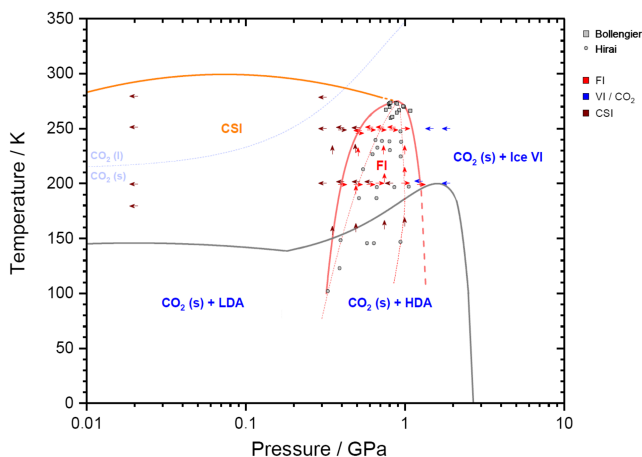


FIG. 10. Comparison of CO<sub>2</sub>/H<sub>2</sub>O phases observed in different types of experiments. The grey data points are selected experiments of Hirai *et al.*<sup>3</sup> and Bollengier *et al.*<sup>4</sup> ↑: isobaric annealing; →: isothermal compression of CS-I; ←: isothermal decompression of ice VI and dry ice. Blue, brown, and red arrows represent CO<sub>2</sub>(s)+ice VI, clathrate hydrate, and filled ice, respectively, and indicate the most abundant component found at this point in the *p/T* plane.

- <sup>1</sup>E. D. Sloan, *Nature* **426**, 353 (2003).
- <sup>2</sup>E. Sloan and C. Kohl, *Clathrate Hydrates of Natural Gases* (CRC Press, 2008).
- <sup>3</sup>H. Hirai, K. Komatsu, M. Honda, T. Kawamura, Y. Yamamoto, and T. Yagi, *J. Chem. Phys.* **133**, 124511 (2010).
- <sup>4</sup>O. Bollengier, M. Choukroun, O. Grasset, E. L. Menn, G. Bellino, Y. Morizet, L. Bezacier, A. Oancea, and G. Tobie, *Geochim. Cosmochim. Acta* **119**, 322 (2013).
- <sup>5</sup>J. Bernard, M. Seidl, E. Mayer, and T. Loerting, *Chem. Phys. Chem.* **13**, 3087 (2012).
- <sup>6</sup>H. Wang, J. Zeuschner, M. Eremets, I. Troyan, and J. Willams, *Sci. Rep.* **6**, 19902 (2016).
- <sup>7</sup>G. Saleh and A. R. Oganov, *Sci. Rep.* **6**, 32486 (2016).
- <sup>8</sup>E. Abramson, O. Bollengier, and J. Brown, *Sci. Rep.* **7**, 821 (2017).
- <sup>9</sup>D. Mahajan, C. E. Taylor, and G. A. Mansoori, *J. Pet. Sci. Eng.* **56**, 1 (2007).
- <sup>10</sup>R. Pellenberg and M. Max, *J. Chem. Ed.* **78**, 896 (2001).
- <sup>11</sup>B. A. Buffett, *Annu. Rev. Earth Planet. Sci.* **28**, 477 (2000).
- <sup>12</sup>S. Takeya, A. Hori, T. Hondoh, and T. Udachin, *J. Phys. Chem. B* **104**, 4164–4168 (2000).
- <sup>13</sup>R. Sakemoto, H. Sakamoto, K. Shiraiwa, R. Ohmura, and T. Uchida, *Cryst. Growth Des.* **10**, 1296 (2010).
- <sup>14</sup>K. Saito, M. Kishimoto, R. Tanaka, and R. Ohmura, *Cryst. Growth Des.* **11**, 295 (2011).
- <sup>15</sup>D. K. Staykova, W. F. Kuhs, A. N. Salamatin, and T. Hansen, *J. Phys. Chem. B* **107**, 10299 (2003).
- <sup>16</sup>J. S. Loveday, R. J. Nelmes, M. Guthrie, D. D. Klug, and J. S. Tse, *Phys. Rev. Lett.* **87**, 215501 (2001).
- <sup>17</sup>J. S. Loveday and R. Nelmes, *Phys. Chem. Chem. Phys.* **10**, 937 (2007).
- <sup>18</sup>R. T. Downst and M. S. Somayazulu, *Acta Crystallogr., Sect. C: Cryst. Struct. Commun.* **54**, 897 (1998).
- <sup>19</sup>B. Kamb, *Science* **150**, 205 (1965).
- <sup>20</sup>C. A. Tulk, S. Machida, D. D. Klug, H. Lu, M. Guthrie, and J. Molaison, *J. Chem. Phys.* **141**, 174503 (2014).

- <sup>21</sup>K. Roettger, A. Endriss, and J. Ihringer, *Acta Cryst. B* **50**, 644–648 (1994).
- <sup>22</sup>D. Londono, W. F. Kuhs, and J. L. Finney, *Nature* **332**, 141 (1988).
- <sup>23</sup>S. Machida, H. Hisako, K. Taro, Y. Yoshitaka, and Y. Takehiko, *J. Chem. Phys.* **129**, 224505 (2008).
- <sup>24</sup>H. Lukman, K. Kenichiro, and T. Hideki, *Phys. Rev. B* **82**, 144105 (2010).
- <sup>25</sup>A. Simon and K. Peters, *Acta Crystallogr., Sect. B: Struct. Sci.* **36**, 2750 (1980).
- <sup>26</sup>E. Mayer and R. Pletzer, *J. Chem. Phys.* **80**, 2939 (1984).
- <sup>27</sup>C. Mitterdorfer, M. Bauer, and T. Loerting, *Phys. Chem. Chem. Phys.* **13**, 19765 (2011).
- <sup>28</sup>C. Mitterdorfer, “Phase changes in CO<sub>2</sub>/H<sub>2</sub>O ices,” Ph.D. thesis, University of Innsbruck, 2014.
- <sup>29</sup>E. F. Burton and W. F. Oliver, *Nature* **135**, 505 (1935).
- <sup>30</sup>T. Loerting, C. Mitterdorfer, M. Bauer, K. Winkel, M. Seidl, P. H. Handle, C. G. Salzmann, E. Mayer, D. T. Bowron, and J. Finney, *Phys. Chem. Chem. Phys.* **13**, 8783 (2011).
- <sup>31</sup>M. S. Elsaesser, I. Kohl, E. Mayer, and T. Loerting, *J. Phys. Chem. B* **111**, 8038 (2007).
- <sup>32</sup>O. Mishima, L. D. Calvert, and E. Whalley, *Nature* **310**, 393 (1984).
- <sup>33</sup>I. Kohl, E. Mayer, and A. Hallbrucker, *Phys. Chem. Chem. Phys.* **3**, 602 (2001).
- <sup>34</sup>O. Mishima, *J. Chem. Phys.* **100**, 5910 (1994).
- <sup>35</sup>K. Winkel, M. S. Elsaesser, E. Mayer, and T. Loerting, *J. Chem. Phys.* **128**, 044510 (2008).
- <sup>36</sup>M. Bernstein, D. Cruikshank, and S. Sandford, *Icarus* **179**, 527 (2005).
- <sup>37</sup>T. Loerting, I. Kohl, C. Salzmann, E. Mayer, and A. Hallbrucker, *J. Chem. Phys.* **116**, 3171 (2002).
- <sup>38</sup>C. G. Salzmann, T. Loerting, I. Kohl, E. Mayer, and A. Hallbrucker, *J. Phys. Chem. B* **106**, 5587 (2002).
- <sup>39</sup>The same process is visible in the 200 K case. However, due to a lower temperature this transition is slower.
- <sup>40</sup>C. Salzmann, T. Loerting, S. Klotz, P. Mirwald, A. Hallbrucker, and E. Mayer, *Phys. Chem. Chem. Phys.* **8**, 386 (2005).
- <sup>41</sup>J. Stern and T. Loerting, *Sci. Rep.* **7**, 3995 (2002).
- <sup>42</sup>Y. P. Handa, D. Klug, and E. Whalley, *Can. J. Chem.* **66**, 919 (1988).
- <sup>43</sup>Traditionally, ice I was considered to exist in two well-defined crystalline forms at ambient pressure: stable hexagonal ice (ice I<sub>h</sub>) and metastable cubic ice (ice I<sub>c</sub>). However, it is becoming increasingly evident that what has been called cubic ice in the past does not have a structure consistent with the cubic crystal system. Instead, it is a stacking-disordered material containing cubic sequences interlaced with hexagonal sequences.<sup>46</sup>
- <sup>44</sup>T. C. Hansen, M. M. Koza, and W. F. Kuhs, *J. Phys.: Condens. Matter* **20**, 285104 (2008).
- <sup>45</sup>T. Malkin, B. Murray, C. Salzmann, V. Molinero, S. Pickering, and T. Whale, *Phys. Chem. Chem. Phys.* **17**, 60 (2015).
- <sup>46</sup>W. Kuhs, D. Bliss, and J. Finney, *J. Phys. Colloq.* **48**(C1), C1-631 (1987).